

Band structures and transmission spectra of piezoelectric superlattices

Weiye Zhang, Zhenxing Liu, and Zhenlin Wang

National Laboratory of Solid State Microstructures and Department of Physics, Nanjing University, Nanjing 210093, China

(Received 29 November 2004; revised manuscript received 11 February 2005; published 26 May 2005)

The polaritonlike excitations in piezoelectric-modulated superlattices are studied systematically by combining the plane wave expansion method and transfer matrix method; these two complementary methods yield the full band structures of the system and mode-coupling information with the external incident waves. Both the band structures and transmission spectra are calculated and analyzed for superlattices made of LiNbO_3 , and the polaritonlike band gap (divided by midgap frequency) of 19% is found in the computed transmission spectra of electromagnetic wave. Furthermore, our study shows that the transmission spectra depend sensitively on the sample thickness and the well defined polaritonlike band gap takes shape only when the number of periods exceeds 10 000. Our results offer a natural explanation as to why previous experiments failed to observe the gap in a sample with 250 periods.

DOI: 10.1103/PhysRevB.71.195114

PACS number(s): 42.25.Gy, 63.20.Ls, 71.36.+c, 77.65.-j

I. INTRODUCTION

With the advancement in nanofabrication technology more and more artificial structures with desired properties are proposed and fabricated. The photonic crystals and phononic crystals are just two examples in this category.¹⁻¹⁶ In solid state physics, it is well known that periodic potential in solids results in electronic band formation due to Bloch theorem, the propagation of electronic waves is thus modulated by the underlying crystal structure. Inspired by the same logic, Yablonoitch and John^{1,2} proposed the concept of photonic crystals (PC) which are dielectric modulated structures in space. Electromagnetic wave also forms band structures in PCs and absolute photonic band gap (PBG) can be created sometimes.³⁻¹⁰ The PBGs are explored to control and manipulate the propagation of electromagnetic waves and form the base for a variety of device applications. Such innovative thinking was further extended to phononic crystals¹¹⁻¹⁴ (PhC) with space modulated elastic structures. Also, PhCs with local-resonator structures were designed and experimentally verified by several groups.^{15,16} The achieved low frequency phononic band gaps (PhBG) can be used to prevent the propagation of low frequency sound wave from noise generators.

Recently, the so-called ionic-type phononic crystal was proposed by Lu *et al.*^{17,18} The structure is made of ferroelectric superlattices with alternately reversed domain structures and piezoelectric constant is modulated due to domain reversal. A simple phenomenological model¹⁷ was devised to mimic the coupling between the long wavelength “optical phonon” of superlattices and electromagnetic wave, an equation set similar to Huang’s equation¹⁹ was derived. In analog to ionic crystals where strong coupling between flat optical phonons and photons favors the creation of polariton band gap, a polaritonlike band gap is also predicted in the ionic-type phononic crystal^{17,18} as a result of coupling between folded “optical phonons” and photons. The relative band gap (band gap divided by mid-gap frequency) was theoretically estimated to be 7%. The reflection coefficient of the superlattice with 250 lattice periods was measured in a waveguide mode, an absorption dip was observed at the frequency near

long wavelength “optical phonon” modes, and the polaritonlike band gap was not verified experimentally.

The ionic-type phononic crystal is unique in the sense that eigenmodes in such superlattices result from the hybridization of “optical phonons” and photons so that both “optical phonons” and photons are forbidden to propagate if an absolute polaritonlike band gap exists. This property makes it possible to control and manipulate the flows of both photons and phonons simultaneously, and new opto-acoustic devices might be designed. For example, high efficient ultrasound generator could be designed by controlling the energy transfer between photons and phonons as they behave like two interdependent degrees of freedom.

Because of the fundamental importance of the concept of manmade polaritonlike crystals and its potential application in the control and manipulation of the propagation of both electromagnetic waves and acoustic waves, several issues need to be elucidated. (1) The superlattice structures split the common acoustic dispersion curve in ferroelectric media into one “acoustic phonon” branch and infinite numbers of “optical phonon” branches. A question arises as whether all “optical phonons” are coupled to the electromagnetic waves? (2) In the phenomenological treatment, the dispersion of “optical phonons” was not considered when mapping the ferroelectric superlattice with piezoelectric modulation into Huang’s equation set, it is of interest to know whether the polaritonlike band gap is sustained when the acoustic band dispersion is taken into account. (3) If there exists a genuine polaritonlike band gap in such piezoelectric superlattice, why the previous experiment failed to detect it in the transmission measurement.¹⁷

All these issues have great impact on the robustness of polaritonlike band gap and phenomenological theory is not enough to address the topics. In this paper, we tackle these issues with two complementary methods: the plane wave method is used to calculate the polaritonlike band structure in infinite superlattices; the transfer matrix method is adopted to analyze the couplings between external incident electromagnetic wave and various modes in finite superlattices. In addition, the transfer matrix method not only presents the directly measurable transmission spectra, but also

offers a cross check for the band structures when used together with the Bloch theorem. Since the physical properties of piezoelectric modulated superlattices are determined by the piezoelectric coefficients which stipulate the couplings between the lattice strain and electric field, the largest coupling is achieved only for certain configurations of field polarization and strain components. In this paper, we consider the two experimental settings below (see Fig. 1) which correspond to the optimized electromechanic coefficients in LiNbO₃. The theoretical analyses and calculated transmission spectra show that the polaritonlike band gap does exist and relative gap can reach 19% for the setting shown in Fig. 1(a). The second important feature we find is the strong dependence of transmission and reflection coefficients on sample thickness, the well defined polariton-like band gaps take shapes only when sample thickness reaches several photon wavelengths which amounts to several ten thousands of lattice periods. The sample thickness considered in Ref. 17 has only 250 periods and is much smaller than photon wavelength, this is the reason why the polariton gap was not detected there. It should be mentioned that the previous plane wave treatment²⁰ made several errors both in introducing the nonlinear transformation in their Eq. (4) and in obtaining the complex wave numbers (see their Fig. 4) which render their results invalid.

The rest of the paper is organized in the following way. In Sec. II, we first derive the coupled equation set which governs the propagation behavior of electromagnetic waves and elastic waves in the piezoelectric superlattices. This equation set is then solved by using two complementary methods, the band structure for infinite long superlattice is obtained both by using the plane wave expansion method and by using the transfer matrix method for cross checking, and the transmission and reflection spectra for finite long superlattice are obtained by using the transfer matrix method. The results on the band structures and transmission spectra are presented in Sec. III, in particular, reasons why the polariton like band gap was not observed in previous experiments are discussed regarding the size dependence of the transmission spectra. The conclusion is drawn in Sec. IV.

II. PLANE WAVE METHOD AND TRANSFER MATRIX METHOD

As we have mentioned in the Introduction, various experimental settings can be designed for the piezoelectric superlattices depending on the field direction, domain polarization, and lattice strain, and they are characterized by different electromechanic coefficients. In order to optimize the electromechanic coefficient, one needs to have settings which correspond to the largest component of the piezoelectric tensor. For LiNbO₃ compound, the two configurations shown in Fig. 1 have the largest (d_{15}) and second largest ($d_{16}=-2d_{22}$) piezoelectric components. Furthermore, the forms of reduced equation sets for the two configurations turn out to be exactly the same except for the effective parameters, thus only the in-plane configuration is discussed in detail below. The piezoelectric superlattices involve the coupling between electric field and lattice strain. For the con-

figuration shown in Fig. 1(a), transverse electric field and lattice displacement are in x axis, the full dynamics of the system is described by the Maxwell equation for electric field $E_x(z, t)$

$$\frac{\partial^2}{\partial z^2} E_x(z, t) = \frac{1}{\epsilon_0 c^2} \frac{\partial^2}{\partial t^2} D_x(z, t), \quad (1)$$

and the vibrational equation for lattice displacement $u_x(z, t)$

$$\rho \frac{\partial^2}{\partial t^2} u_x(z, t) = \frac{\partial}{\partial z} Z_5(z, t). \quad (2)$$

Here, ϵ_0 is the vacuum permittivity and c is the light velocity in vacuum, ρ is the mass density of LiNbO₃. This equation set does not form a complete set of equations and has to be supplemented by state equations for electric displacement vector $D_x(z, t)$ and stress component $Z_5(z, t)$. For the piezoelectric crystal LiNbO₃ under consideration, the piezoelectric tensor takes the form

$$(d_{ij}) = \begin{pmatrix} 0 & 0 & 0 & 0 & d_{15} & -2d_{22} \\ -d_{22} & d_{22} & 0 & d_{15} & 0 & 0 \\ d_{31} & d_{31} & d_{33} & 0 & 0 & 0 \end{pmatrix}. \quad (3)$$

For the transverse electric field in x axis, the nonzero components of piezoelectric tensor are d_{15} and $d_{16}=-2d_{22}$, and they couple to the stress components Z_5 and Z_6 . Thus the electric displacement $D_x(z, t)$ and strain components e_5 and e_6 are given by

$$D_x(z, t) = d_{15}(z)Z_5(z, t) + d_{16}(z)Z_6(z, t) + \epsilon_0 \epsilon E_x(z, t), \quad (4a)$$

$$e_5(z, t) = s_{55}Z_5(z, t) + s_{56}Z_6(z, t) + d_{15}(z)E_x(z, t), \quad (4b)$$

$$e_6(z, t) = s_{65}Z_5(z, t) + s_{66}Z_6(z, t) + d_{16}(z)E_x(z, t), \quad (4c)$$

where s_{ij} 's are bulk moduli and ϵ is the dielectric constant of LiNbO₃. In writing down these state equations, a convention has been used that the polarization direction of ferroelectric domains is set as z axis. Note that strain components are related to lattice displacement by $e_5 = \partial u_x(z, t) / \partial z + \partial u_z(z, t) / \partial x = \partial u_x(z, t) / \partial z$ and $e_6 = \partial u_x(z, t) / \partial y + \partial u_y(z, t) / \partial x = 0$ since only $u_x(z, t) \neq 0$ for the configuration shown in Fig. 1(a). From these relationships, the electric displacement $D_x(z, t)$ and stress components Z_5 and Z_6 can be obtained in terms of electric field $E_x(z, t)$ and lattice displacement $u_x(z, t)$

$$D_x(z, t) = \frac{\bar{d}_{15}(z)}{\bar{s}_{55}} \partial u_x(z, t) / \partial z + \epsilon_0 (\epsilon - \Delta \epsilon) E_x(z, t), \quad (5a)$$

$$Z_5(z, t) = \frac{1}{\bar{s}_{55}} \frac{\partial}{\partial z} u_x(z, t) - \frac{\bar{d}_{15}(z)}{\bar{s}_{55}} E_x(z, t), \quad (5b)$$

$$Z_6(z,t) = \frac{1}{\bar{s}_{56}} \frac{\partial}{\partial z} u_x(z,t) - \frac{\bar{d}_{16}(z)}{\bar{s}_{66}} E_x(z,t). \quad (5c)$$

In Eq. (5), $\Delta\epsilon$ is the correction to dielectric constant from the piezoelectric contribution and it has the form

$$\Delta\epsilon = \frac{1}{\epsilon_0} \left[\frac{d_{15}^2}{\bar{s}_{55}} + \frac{d_{16}^2}{\bar{s}_{66}} + d_{15}d_{16} \left(\frac{1}{\bar{s}_{56}} + \frac{1}{\bar{s}_{65}} \right) \right]. \quad (6)$$

Note that the above simple and compact expressions are made possible after we have introduced the reduced bulk moduli \bar{s}_{ij}

$$\frac{1}{\bar{s}_{55}} = \frac{s_{66}}{s_{55}s_{66} - s_{56}s_{65}}, \quad (7a)$$

$$\frac{1}{\bar{s}_{66}} = \frac{s_{55}}{s_{55}s_{66} - s_{56}s_{65}}, \quad (7b)$$

$$\frac{1}{\bar{s}_{56}} = \frac{-s_{65}}{s_{55}s_{66} - s_{56}s_{65}}, \quad (7c)$$

$$\frac{1}{\bar{s}_{65}} = \frac{-s_{56}}{s_{55}s_{66} - s_{56}s_{65}}, \quad (7d)$$

and reduced piezoelectric coefficients $\bar{d}_{15}(z)$, $\bar{d}_{16}(z)$

$$\bar{d}_{15}(z) = d_{15}(z) + d_{16}(z) \frac{\bar{s}_{55}}{\bar{s}_{65}}, \quad (8a)$$

$$\bar{d}_{16}(z) = d_{16}(z) + d_{15}(z) \frac{\bar{s}_{66}}{\bar{s}_{56}}. \quad (8b)$$

The bulk moduli are polarization independent and they are constants throughout samples of superlattice, but the piezoelectric coefficients are polarization dependent and they change their signs for oppositely polarized domains, this is the reason why we write explicitly the piezoelectric coefficients as space dependent functions. Substituting the expressions for dielectric displacement $D_x(z,t)$ [Eq. (5a)] and stress component Z_5 [Eq. (5b)] into Eq. (1) and Eq. (2), and defining the sound velocity in the media $c_s^2 = 1/\rho\bar{s}_{55}$, one finally gets a set of coupled equations for electric field $E_x(z,t)$ and lattice displacement $u_x(z,t)$

$$\frac{\bar{\epsilon}}{c^2} \frac{\partial^2}{\partial t^2} E_x(z,t) = \frac{\partial^2}{\partial z^2} E_x(z,t) - \frac{\bar{d}_{15}(z)}{\epsilon_0 c^2 \bar{s}_{55}} \frac{\partial^3}{\partial t^2 \partial z} u_x(z,t), \quad (9a)$$

$$\frac{1}{c_s^2} \frac{\partial^2}{\partial t^2} u_x(z,t) = \frac{\partial^2}{\partial z^2} u_x(z,t) - \frac{\partial}{\partial z} \bar{d}_{15}(z) E_x(z,t). \quad (9b)$$

$\bar{\epsilon} = \epsilon - \Delta\epsilon$ is the effective dielectric constant. To facilitate the numerical analysis, it is customary to write the equation set into a dimensionless form. This can be done after introducing the following dimensionless variables (with a bar on the top) through $z = \bar{z}L/2\pi$, $u_x(z,t) = \bar{u}_x(\bar{z},t)L/2\pi$, and $\bar{E}_x(\bar{z},t) = \bar{d}_{15} E_x(z,t)$. L is the lattice constant of

piezoelectric superlattice and is the sum of two oppositely polarized domains. $\bar{d}_{15}(\bar{z}) = |\bar{d}_{15}|\theta(\bar{z})$ and $\theta(\bar{z}) = \pm 1$ denote the left and right polarized domains. Using these new variables, the dimensionless form of the equation set becomes

$$\left(\frac{L}{2\pi c_s} \right)^2 \frac{\partial^2}{\partial t^2} \bar{E}_x(\bar{z},t) = \frac{c^2}{\bar{\epsilon} c_s^2} \frac{\partial^2}{\partial \bar{z}^2} \bar{E}_x(\bar{z},t) - \frac{\bar{d}_{15}^2}{\epsilon_0 \bar{\epsilon} s_{55}} \theta(\bar{z}) \times \left(\frac{L}{2\pi c_s} \right)^2 \frac{\partial^2}{\partial t^2} \frac{\partial}{\partial \bar{z}} \bar{u}_x(\bar{z},t), \quad (10a)$$

$$\left(\frac{L}{2\pi c_s} \right)^2 \frac{\partial^2}{\partial t^2} \bar{u}_x(\bar{z},t) = \frac{\partial^2}{\partial \bar{z}^2} \bar{u}_x(\bar{z},t) - \frac{\partial}{\partial \bar{z}} [\theta(\bar{z}) \bar{E}_x(\bar{z},t)]. \quad (10b)$$

To calculate the band structures and transmission spectra, it is often convenient to work in the frequency space. After making the Fourier transformation to frequency (ω) space, the equation set reads

$$\left(\frac{\omega L}{2\pi c_s} \right)^2 \bar{E}_x(\bar{z},\omega) = - \frac{c^2}{\bar{\epsilon} c_s^2} \frac{\partial^2}{\partial \bar{z}^2} \bar{E}_x(\bar{z},\omega) - \frac{\bar{d}_{15}^2}{\epsilon_0 \bar{\epsilon} s_{55}} \theta(\bar{z}) \times \left(\frac{\omega L}{2\pi c_s} \right)^2 \frac{\partial}{\partial \bar{z}} \bar{u}_x(\bar{z},\omega), \quad (11a)$$

$$\left(\frac{\omega L}{2\pi c_s} \right)^2 \bar{u}_x(\bar{z},\omega) = - \frac{\partial^2}{\partial \bar{z}^2} \bar{u}_x(\bar{z},\omega) + \frac{\partial}{\partial \bar{z}} [\theta(\bar{z}) \bar{E}_x(\bar{z},\omega)]. \quad (11b)$$

Here $E_x(\bar{z},\omega)$ and $u_x(\bar{z},\omega)$ are the Fourier transformed quantities of $E_x(\bar{z},t)$ and $u_x(\bar{z},t)$. From Eqs. (11a) and (11b) one notices that the dynamics of piezoelectric superlattices is characterized by two dimensionless material parameters, one is the ratio of velocity squared between the light and sound in the media $\alpha = c^2/\bar{\epsilon}c_s^2$, another is the electromechanic coefficient $\beta = \bar{d}_{15}^2/\epsilon_0 \bar{\epsilon} s_{55}$ which describes the efficiency of energy transfer between electromagnetic energy and lattice vibrational energy. The eigenspectra of superlattices are given in terms of the reduced frequency $\bar{\omega} = \omega L/2\pi c_s$. An estimation of these parameters gives us a rough idea on the strength of coupling between electromagnetic wave and sound wave in different experimental settings. For superlattice composed of LiNbO₃ ferroelectric materials,²¹ $\alpha = 1.6 \times 10^8$, $\beta = 0.5923$ for Fig. 1(a) and $\alpha = 1.28 \times 10^8$, $\beta = 0.2222$ for Fig. 1(b), thus the coupling between photons and phonons is strongest in case (a). Note that the photon velocity is four orders of magnitude higher than the sound velocity, their wavelengths set two different characteristic length scales in the system. In the following, we develop the plane wave expansion method and transfer matrix method from Eqs. (11a) and (11b) to obtain the band structures and the transmission and reflection spectra of superlattices.

Plane wave expansion method. For the periodically modulated piezoelectric superlattices, the electric field $\bar{E}_x(\bar{z},\bar{\omega})$ and lattice displacement $\bar{u}_x(\bar{z},\bar{\omega})$ satisfy the Bloch theorem.

For scaled superlattices under discussion, the real space translational vector is $\bar{R}_l=2\pi l$, the corresponding translational vector in the reciprocal space is $K_n=n$ with l, n as integers. Thus, $\bar{E}_x(\bar{z}, \bar{\omega})$ and $\bar{u}_x(\bar{z}, \bar{\omega})$ for a given wave vector $\bar{k}=kL/2\pi$ and $\bar{\omega}$ can be expanded in the reciprocal space as follows:

$$\bar{E}_x(\bar{z}, \bar{\omega}) = \sum_{K_n} G(\bar{k} + K_n, \bar{\omega}) \exp[i(\bar{k} + K_n)\bar{z}], \quad (12a)$$

$$\bar{u}_x(\bar{z}, \bar{\omega}) = \sum_{K_n} (-i)H(\bar{k} + K_n, \bar{\omega}) \exp[i(\bar{k} + K_n)\bar{z}]. \quad (12b)$$

A prefactor $(-i)$ is added in Eq. (12b) in order to make the coefficients of the matrix equation below all real. The differential equation set (11a) and (11b) is then transformed into a matrix equation

$$\begin{aligned} \bar{\omega}^2 G(\bar{k} + K_n, \bar{\omega}) &= \alpha(\bar{k} + K_n)^2 G(\bar{k} + K_n, \bar{\omega}) \\ &\quad - \bar{\omega}^2 \beta \sum_{K_m} (\bar{k} + K_m) \theta(K_n - K_m) \\ &\quad \times H(\bar{k} + K_m, \bar{\omega}), \end{aligned} \quad (13a)$$

$$\begin{aligned} \bar{\omega}^2 H(\bar{k} + K_n, \bar{\omega}) &= (\bar{k} + K_n)^2 H(\bar{k} + K_n, \bar{\omega}) \\ &\quad - (\bar{k} + K_n) \sum_{K_m} \theta(K_n - K_m) G(\bar{k} + K_m, \bar{\omega}). \end{aligned} \quad (13b)$$

$\theta(K_n)$ is the Fourier component of $\theta(\bar{z})$ and is given by

$$\theta(K_n) = \begin{cases} \frac{(\bar{L}_+ - \pi)}{\pi} & \text{if } n = 0, \\ \frac{2 \sin(n\bar{L}_+/2)}{n\pi} & \text{if } n \neq 0, \end{cases} \quad (14)$$

and $\bar{L}_\pm = 2\pi L_\pm/L$ are the scaled layer thicknesses for the left and right polarized domains.

The matrix equation set (13a) and (13b) has the advantage that it does not involve the derivative of $\delta(\bar{z})$ function, thus it is numerically stable. But this advantage is achieved at the expense of reducing the original eigenvalue problem to a noneigenvalue problem since the frequency now appears on the right side of Eq. (13a), an alternative numerical method has to be devised to find its solutions. We adopt the root finding program codes originally used in the multiple scattering method, for a given wave vector \bar{k} we first diagonalize the matrix with certain order in reciprocal space, by counting the positive eigenvalues for the consecutive frequencies all the eigenvalues for a given \bar{k} can be picked up, thus yield the band structures of piezoelectrically modulated superlattices.

We have also explored other representation of differential equation set (11a) and (11b) to check the numerical feasibility. One possibility is to substitute Eq. (11b) into Eq. (11a) to eliminate the right frequency dependent part of Eq. (11a), and to treat the newly obtained equation and old Eq. (11b) as

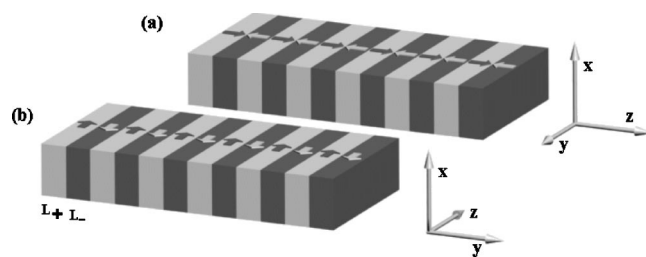


FIG. 1. The schematic setups of piezoelectric superlattices. The electric field and vibrational displacement are taken as x axis; L_+ and L_- denote the widths and arrows refer to the polarization directions of domains. The polarization is (a) perpendicular to the domain; (b) within the domain.

two independent equations. However, this equation set involves the derivative of δ function in space and numerical procedure turns out to be divergent. Another possibility is to rearrange the equation set (11a) and (11b) into the differential equations with respect to the electric field and stress component $Z_5(\bar{z}) = d\bar{u}_x/d\bar{z} - \theta(\bar{z})\bar{E}_x$ as two independent functions,²⁰ but this transformation involves $\theta(\bar{z})$ which takes $\theta(\bar{z}) = \pm 1$ for left and right polarized domains, the eigenvalues obtained do not correspond to those obtained from Eqs. (11a) and (11b), this is also the reason why the gap calculated in Ref. 20 is much smaller than what we obtained in this paper.

Transfer matrix method. To cross check the band structures obtained in the plane wave expansion method and to analyze the mode coupling with external incident waves, the transfer matrix method is also employed to solve the band structures and transmission spectra of piezoelectric superlattices. To do so, we first solve the eigenvalues and eigenvectors in homogeneously polarized domain. For the left polarized domain [$\theta(\bar{z})=1$], by substituting Eq. (11b) into Eq. (11a), Eqs. (11a) and (11b) can be rearranged into the following simple form:

$$\bar{\omega}^2 \bar{E}_x(\bar{z}, \bar{\omega}) = -\alpha \frac{\partial^2}{\partial \bar{z}^2} \bar{E}_x(\bar{z}, \bar{\omega}) - \beta \frac{\partial^2}{\partial \bar{z}^2} \bar{E}_x(\bar{z}, \bar{\omega}) + \beta \frac{\partial^3}{\partial \bar{z}^3} \bar{u}_x(\bar{z}, \bar{\omega}), \quad (15a)$$

$$\bar{\omega}^2 \bar{u}_x(\bar{z}, \bar{\omega}) = -\frac{\partial^2}{\partial \bar{z}^2} \bar{u}_x(\bar{z}, \bar{\omega}) + \frac{\partial}{\partial \bar{z}} \bar{E}_x(\bar{z}, \bar{\omega}). \quad (15b)$$

Since the propagation modes in homogeneous media have the plane wave type

$$\bar{E}_x(\bar{z}, \bar{\omega}) = \bar{E}_x(\bar{k}, \bar{\omega}) \exp(i\bar{k}\bar{z}), \quad (16a)$$

$$\bar{u}_x(\bar{z}, \bar{\omega}) = \bar{u}_x(\bar{k}, \bar{\omega}) \exp(i\bar{k}\bar{z}), \quad (16b)$$

the dispersion relation is determined by the following equation set:

$$\bar{\omega}^2 \bar{E}_x(\bar{k}, \bar{\omega}) = (\alpha + \beta) \bar{k}^2 \bar{E}_x(\bar{k}, \bar{\omega}) - i\beta \bar{k}^3 \bar{u}_x(\bar{k}, \bar{\omega}), \quad (17a)$$

$$\bar{\omega}^2 \bar{u}_x(\bar{k}, \bar{\omega}) = \bar{k}^2 \bar{u}_x(\bar{k}, \bar{\omega}) + i \bar{k} \bar{E}_x(\bar{k}, \bar{\omega}). \quad (17b)$$

Thus there exist four propagation modes for a given frequency $\bar{\omega}$, their wave numbers and eigenfunctions are listed below:

$$\begin{pmatrix} \bar{E}_x(\bar{k}, \bar{\omega}) \\ \bar{u}_x(\bar{k}, \bar{\omega}) \end{pmatrix} = \frac{1}{\sqrt{c_+^2 + (c_+^2 - 1)^2 \bar{\omega}^2}} \begin{pmatrix} (c_+^2 - 1) \bar{\omega} \\ ic_+ \end{pmatrix} \exp(i \bar{\omega} \bar{z} / c_+) \quad (18a)$$

for $k = \bar{\omega} / c_+$,

$$\begin{pmatrix} \bar{E}_x(\bar{k}, \bar{\omega}) \\ \bar{u}_x(\bar{k}, \bar{\omega}) \end{pmatrix} = \frac{1}{\sqrt{c_-^2 + (c_-^2 - 1)^2 \bar{\omega}^2}} \begin{pmatrix} (c_-^2 - 1) \bar{\omega} \\ ic_- \end{pmatrix} \exp(i \bar{\omega} \bar{z} / c_-) \quad (18b)$$

for $k = \bar{\omega} / c_-$,

$$\begin{pmatrix} \bar{E}_x(\bar{k}, \bar{\omega}) \\ \bar{u}_x(\bar{k}, \bar{\omega}) \end{pmatrix} = \frac{1}{\sqrt{c_+^2 + (c_+^2 - 1)^2 \bar{\omega}^2}} \begin{pmatrix} (c_+^2 - 1) \bar{\omega} \\ -ic_+ \end{pmatrix} \times \exp(-i \bar{\omega} \bar{z} / c_+) \quad (18c)$$

for $k = -\bar{\omega} / c_+$,

$$\begin{pmatrix} \bar{E}_x(\bar{k}, \bar{\omega}) \\ \bar{u}_x(\bar{k}, \bar{\omega}) \end{pmatrix} = \frac{1}{\sqrt{c_-^2 + (c_-^2 - 1)^2 \bar{\omega}^2}} \begin{pmatrix} (c_-^2 - 1) \bar{\omega} \\ -ic_- \end{pmatrix} \times \exp(-i \bar{\omega} \bar{z} / c_-) \quad (18d)$$

for $k = -\bar{\omega} / c_-$.

Here $c_{\pm} = \sqrt{0.5[(\alpha + \beta + 1) \pm \sqrt{(\alpha + \beta + 1)^2 - 4\alpha}]}$ are the reduced velocities of electromagnetic wave and sound wave in the media scaled by c_s , first two modes correspond to the electromagnetic wave and sound wave propagating to the left while the last two correspond to those propagating to the right. Similarly, the eigenvalues and eigenfunctions in the right polarized domain can also be derived, their expressions are obtained by replacing c_{\pm} by $-c_{\pm}$ while keeping the phase factors intact.

The general solutions in the left and right polarized domains can be expressed in terms of the above eigenfunctions. Using the boundary conditions that the electric field, lattice displacement, the derivative of electric field (magnetic field), and stress component are continuous across the domain interface, one can define the transfer matrix in each domain which relates the fields and their derivatives at the two sides of a domain

$$\begin{pmatrix} \bar{E}_x(\bar{L}_{\pm}, \bar{\omega}) \\ \bar{u}_x(\bar{L}_{\pm}, \bar{\omega}) \\ \bar{E}'_x(\bar{L}_{\pm}, \bar{\omega}) \\ \bar{u}'_x(\bar{L}_{\pm}, \bar{\omega}) \mp \bar{E}_x(\bar{L}_{\pm}, \bar{\omega}) \end{pmatrix} = M(\bar{L}_{\pm}, \bar{\omega}) \times \begin{pmatrix} \bar{E}_x(\bar{0}, \bar{\omega}) \\ \bar{u}_x(\bar{0}, \bar{\omega}) \\ \bar{E}'_x(\bar{0}, \bar{\omega}) \\ \bar{u}'_x(\bar{0}, \bar{\omega}) \mp \bar{E}_x(\bar{0}, \bar{\omega}) \end{pmatrix}. \quad (19)$$

The detailed expressions of transfer matrices $M(\bar{L}_{\pm}, \bar{\omega})$ are listed in the Appendix. Here upper and lower signs denote the left and right polarized domains. The transfer matrix of a superlattice can be obtained by successive application of $M(\bar{L}_{\pm}, \bar{\omega})$ using the sequence depicting superlattice configuration. This forms the basis to study the band structures and transmission spectra of the superlattices. For example, we can also study the band structures using the Bloch theorem. In this case, we need to solve the following matrix equation:

$$M(\bar{L}_+, \bar{\omega}) M(\bar{L}_-, \bar{\omega}) = \exp(i \bar{k} \bar{L}) I, \quad (20)$$

with I denoting the 4×4 unit matrix.

With the analytic expressions of the transfer matrix for the left and right polarized domains, it is easy to study the transmission and reflection spectra of a finite superlattice. For a finite superlattice with NP number of periods, the transfer matrix of the superlattice is given by

$$M = [M(\bar{L}_+, \bar{\omega}) M(\bar{L}_-, \bar{\omega})]^{NP}. \quad (21)$$

For the transverse vibrational mode illustrated in Fig. 1, only the electromagnetic waves are coupled out since the transverse elastic modulus of air is nearly zero. The transmission t and reflection r amplitudes can be expressed in terms of matrix elements M_{ij} as follows:

$$t = \frac{2M_{42}}{M_{42}[(M_{11} + f_p M_{13}) + f_p^{-1}(M_{31} + f_p M_{33})] - (M_{12} + f_p^{-1} M_{32})(M_{41} + f_p M_{43})}, \quad (22a)$$

$$r = \frac{M_{42}[(M_{11} + f_p M_{13}) - f_p^{-1}(M_{31} + f_p M_{33})] - (M_{12} - f_p^{-1} M_{32})(M_{41} + f_p M_{43})}{M_{42}[(M_{11} + f_p M_{13}) + f_p^{-1}(M_{31} + f_p M_{33})] - (M_{12} + f_p^{-1} M_{32})(M_{41} + f_p M_{43})}, \quad (22b)$$

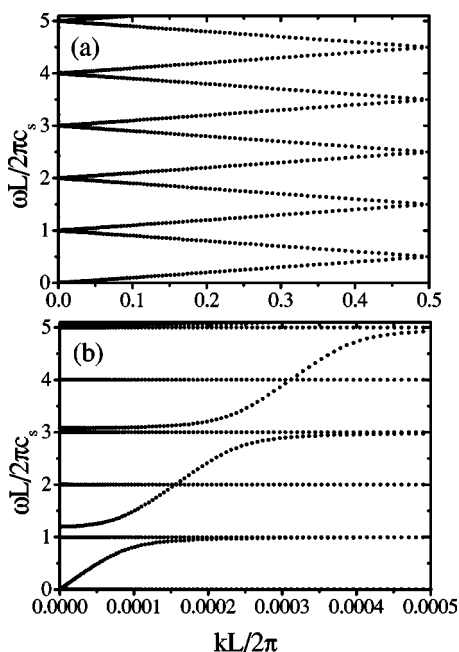


FIG. 2. The polaritonlike band structures of configuration (a) using the plane wave expansion method. The material parameters are listed in text and $\bar{L}_+ = \bar{L}_- = \pi$. (a) For whole Brillouin zone. (b) Near the center of Brillouin zone.

and the parameter $f_p = ic_s \bar{\omega} / c$. The experimentally measured transmission and reflection spectra are given by $T = |t|^2$ and $R = |r|^2$, they satisfy the energy conservation law $R + T = 1$ if no dissipation exists.

III. NUMERICAL RESULTS AND DISCUSSIONS

The band structures of polaritonlike modes can be obtained easily from the matrix equation set (13a) and (13b) based on the plane wave expansion method. Typical results are illustrated in Fig. 2 for configuration (a), where equal widths ($\bar{L}_+ = \bar{L}_- = \pi$) are assumed for left and right polarized domains. Figure 2(a) shows the overall band structure in whole Brillouin zone, the dispersion relation can be viewed as simply folding the dispersion relation of acoustic wave in homogeneous media, and the proposed polaritonlike band gap is not visible in the figure. The fact that $c / \sqrt{\epsilon} c_s = \sqrt{\alpha} \approx 10^4$ reminds us that a significant coupling takes place only near the center of Brillouin zone. This part of the dispersion curves is enlarged and replotted in Fig. 2(b). Several points are worth mentioning concerning the band structure: (1) Besides the lowest polaritonlike band gap theoretically predicted in Ref. 17, here we find additional polaritonlike band gaps when $\omega L / 2\pi c_s$ equals odd integers though the sizes of band gaps decrease rapidly as middle gap frequency increases. (2) Unlike the usual concept of band gap where no eigenmodes can propagate within the gap range, here there obviously exists a branch of “optical phonon” passing through the complete band gap range. Therefore, the existence of proposed band gap is not guaranteed unless the above mentioned “optical phonon” branch is ex-

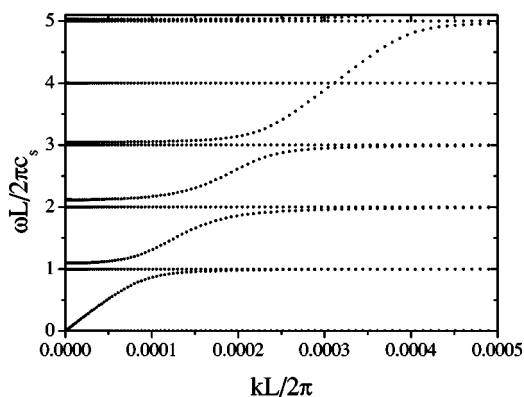


FIG. 3. The polaritonlike band structures of configuration (a) near the center of Brillouin zone using the plane wave expansion method. The material parameters are the same as in Fig. 2, $\bar{L}_+ = 0.5\pi$; $\bar{L}_- = 1.5\pi$.

actly decoupled from the rest of modes even in the presence of boundary. The plane wave expansion method and those perturbation methods previously adopted¹⁸ certainly cannot address this issue. (3) The polaritonlike band gaps also open up at $\omega L / 2\pi c_s = \text{even integers}$ if thicknesses of left and right polarized domains are different [see Eq. (14)]. This is so because the parity symmetry is then broken when $\bar{L}_+, \bar{L}_- \neq \pi$, but all gap sizes are drastically reduced due to the reduced Fourier coefficients of piezoelectric functions. An typical example is shown in Fig. 3 where the widths for left and right polarized domains are taken as $\bar{L}_+ = 0.5\pi$ and $\bar{L}_- = 1.5\pi$, respectively.

To cross check the band structures calculated using the plane wave expansion method, the band structures of configuration (1a) are also computed using Eq. (20) based on the transfer matrix method and Bloch theorem. The same results are found and presented in Fig. 4. The solid circles represent the real wave vector for pass bands while the solid triangles represent the purely imaginary wave vector for forbidden gaps. Figure 4(a) plots the wave vectors for the whole Brillouin zone while Fig. 4(b) is an enlarged portion near the Brillouin center. For a given frequency, the transfer matrix method yields either a real wave vector for the propagation mode or a purely imaginary wave vector for the forbidden mode which describes the attenuation of corresponding mode. Those vertical lines in Fig. 4(b) correspond to the decoupled “optical phonon” branches whose properties deserves further investigation. These band structures are exactly the same as those presented in Fig. 2.

To elucidate the nature of those “optical phonon” branches within the gaps, we also studied the transmission and reflection spectra of finite superlattices using the generalized transfer matrix method described in the last section. For the specific configuration presented in Fig. 1, both electromagnetic wave and lattice wave are transverse waves and only the electromagnetic wave is coupled out. Contrary to the conventional wisdom that tens to hundreds of lattice periods for a superlattice should be good enough to reproduce its bulk behavior, here the piezoelectric superlattice is characterized by two hugely different length scales, i.e., the

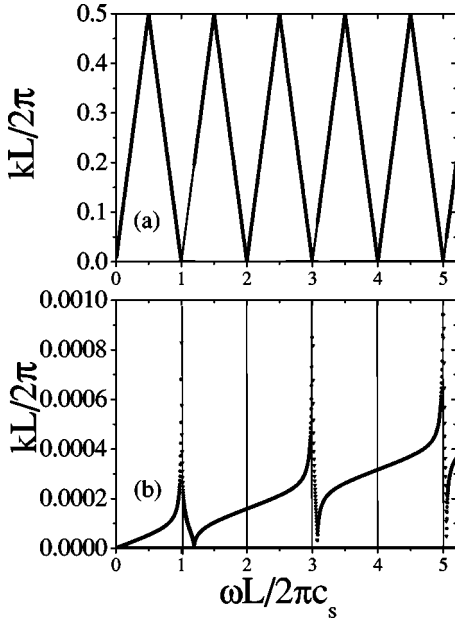


FIG. 4. The polaritonlike band structures of configuration (a) using the transfer matrix method. The material parameters are listed in text and $\bar{L}_+ = \bar{L}_- = \pi$. (a) For whole Brillouin zone. (b) Near the center of Brillouin zone.

wavelengths of photon and phonon. As the phonon wavelength at polariton band gap is comparable to the lattice constant, the photon wavelength must be ten thousand times that of lattice constant. For comparison, the transmission coefficients are shown in Fig. 5 for a different number of lattice periods (NP). The transmission spectra change dramatically with the sample thickness when it is much smaller than the photon wavelength, and well defined polaritonlike band gaps appear only when the sample thickness reaches several photon wavelengths. These results also show that the in-gap “op-

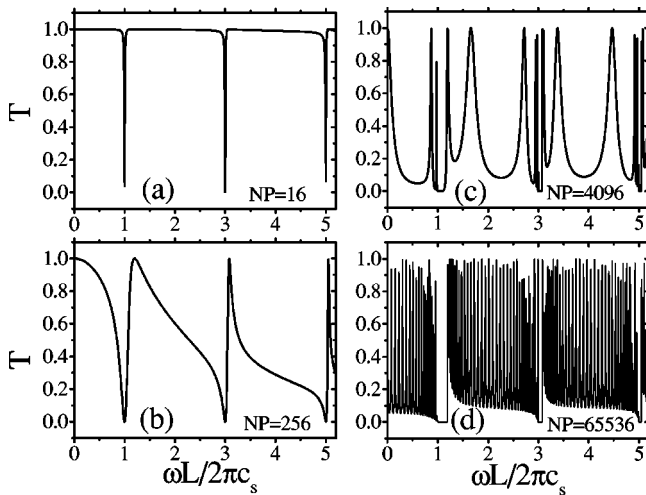


FIG. 5. Transmission coefficients for equal-width piezoelectric superlattices with various sample thicknesses in unit of periods. (a) 16 periods; (b) 256 periods; (c) 4096 periods; (d) 65536 periods. Since reflection and transmission coefficients satisfy the sum rule, only transmission coefficients are shown.

tical phonon” modes in Fig. 2 do decouple from the polaritonlike modes for the configurations shown in Fig. 1, which makes the polaritonlike band gaps genuine. From the transmission spectrum plotted in Fig. 5(d), the relative gaps (gap divided by midgap frequency) are 19%, 2.5%, and 1% for the 1st, 2nd, and 3rd gap, respectively. This should be compared with Ref. 17 where the first gap was predicted and relative gap was estimated to be 7%. Note that the rapid oscillations within the pass band of spectra are due to Fabry-Pérot interference effect in the samples. These calculated transmission and reflection spectra also give an explanation as why the gap was not detected in the previous experiment¹⁷ with sample of 250 lattice periods. Because the sample thickness is far smaller than the photon wavelength, no well defined polaritonlike band gap has taken the shape.

The above study can also be carried out for other transverse and longitudinal acoustic phonon modes and same conclusions can be made. Due to the much smaller coupling constant β , the polaritonlike band gap is much smaller and will not be discussed here in detail.

IV. CONCLUSION

In summary, we have clarified in this paper several issues concerning the existence of the polaritonlike band gap in piezoelectric superlattices. The “optical phonon” branch within the band gap is completely decoupled from external electromagnetic wave and relative gap can be as large as 19%. Our results offer a natural explanation as to why previous experiments failed to observe the gap in a sample with 250 periods.

ACKNOWLEDGMENTS

This work was supported in part by the key research project in “Climbing Program” by the National Science and Technology Commission of China. W.Z. wishes to acknowledge partial financial support from the National Natural Science Foundation of China (NNSFC) under Grant No. 10474040, 19934003, and “Excellent Youth Foundation” [10025419]; Z.W. wishes to acknowledge partial financial support from the NNSFC under Grant Nos. 10174031 and 90101030.

APPENDIX: TRANSFER MATRICES FOR TWO POLARIZED DOMAINS

$c_{\pm} = \sqrt{0.5[(\alpha + \beta + 1) \pm \sqrt{(\alpha + \beta + 1)^2 - 4\alpha}]}$ are the reduced velocities for photons and phonons, respectively. $\bar{\omega} = \omega L / 2\pi c_s$; $\bar{L}_{\pm} = 2\pi L_{\pm} / L$. The upper and lower subindices represent two polarized domains:

$$M(\bar{L}_{\pm}, \bar{\omega}, 1, 1) = \frac{1}{(c_+^2 - c_-^2)} \left[c_-^2 (c_+^2 - 1) \cos \frac{\bar{\omega} \bar{L}_{\pm}}{c_+} - c_+^2 (c_-^2 - 1) \cos \frac{\bar{\omega} \bar{L}_{\pm}}{c_-} \right], \quad (\text{A1})$$

$$M(\bar{L}_{\pm}, \bar{\omega}, 1, 2) = \mp \frac{(c_+^2 - 1)(c_-^2 - 1)\bar{\omega}}{(c_+^2 - c_-^2)} \left[c_+ \sin \frac{\bar{\omega}\bar{L}_{\pm}}{c_+} - c_- \sin \frac{\bar{\omega}\bar{L}_{\pm}}{c_-} \right], \quad (\text{A2})$$

$$M(\bar{L}_{\pm}, \bar{\omega}, 1, 3) = \frac{c_+c_-}{(c_+^2 - c_-^2)\bar{\omega}} \left[c_-(c_+^2 - 1) \sin \frac{\bar{\omega}\bar{L}_{\pm}}{c_+} - c_+(c_-^2 - 1) \sin \frac{\bar{\omega}\bar{L}_{\pm}}{c_-} \right], \quad (\text{A3})$$

$$M(\bar{L}_{\pm}, \bar{\omega}, 1, 4) = \frac{\pm(c_+^2 - 1)(c_-^2 - 1)}{(c_+^2 - c_-^2)} \left[\cos \frac{\bar{\omega}\bar{L}_{\pm}}{c_+} - \cos \frac{\bar{\omega}\bar{L}_{\pm}}{c_-} \right], \quad (\text{A4})$$

$$M(\bar{L}_{\pm}, \bar{\omega}, 2, 1) = \mp \frac{c_+c_-}{(c_+^2 - c_-^2)\bar{\omega}} \left[c_- \sin \frac{\bar{\omega}\bar{L}_{\pm}}{c_+} - c_+ \sin \frac{\bar{\omega}\bar{L}_{\pm}}{c_-} \right], \quad (\text{A5})$$

$$M(\bar{L}_{\pm}, \bar{\omega}, 2, 2) = \frac{-1}{(c_+^2 - c_-^2)} \left[c_+^2(c_-^2 - 1) \cos \frac{\bar{\omega}\bar{L}_{\pm}}{c_+} - c_-^2(c_+^2 - 1) \cos \frac{\bar{\omega}\bar{L}_{\pm}}{c_-} \right], \quad (\text{A6})$$

$$M(\bar{L}_{\pm}, \bar{\omega}, 2, 3) = \frac{\pm c_+^2 c_-^2}{(c_+^2 - c_-^2)\bar{\omega}^2} \left[\cos \frac{\bar{\omega}\bar{L}_{\pm}}{c_+} - \cos \frac{\bar{\omega}\bar{L}_{\pm}}{c_-} \right], \quad (\text{A7})$$

$$M(\bar{L}_{\pm}, \bar{\omega}, 2, 4) = -\frac{1}{(c_+^2 - c_-^2)\bar{\omega}} \left[c_+(c_-^2 - 1) \sin \frac{\bar{\omega}\bar{L}_{\pm}}{c_+} - c_-(c_+^2 - 1) \sin \frac{\bar{\omega}\bar{L}_{\pm}}{c_-} \right], \quad (\text{A8})$$

$$M(\bar{L}_{\pm}, \bar{\omega}, 3, 1) = -\frac{\bar{\omega}}{c_+c_-(c_+^2 - c_-^2)} \left[c_+^3(c_-^2 - 1) \sin \frac{\bar{\omega}\bar{L}_{\pm}}{c_+} - c_-^3(c_+^2 - 1) \sin \frac{\bar{\omega}\bar{L}_{\pm}}{c_-} \right], \quad (\text{A9})$$

$$M(\bar{L}_{\pm}, \bar{\omega}, 3, 2) = \frac{\mp(c_+^2 - 1)(c_-^2 - 1)\bar{\omega}^2}{(c_+^2 - c_-^2)} \left[\cos \frac{\bar{\omega}\bar{L}_{\pm}}{c_+} - \cos \frac{\bar{\omega}\bar{L}_{\pm}}{c_-} \right], \quad (\text{A10})$$

$$M(\bar{L}_{\pm}, \bar{\omega}, 3, 3) = \frac{1}{(c_+^2 - c_-^2)} \left[c_-^2(c_+^2 - 1) \cos \frac{\bar{\omega}\bar{L}_{\pm}}{c_+} - c_+^2(c_-^2 - 1) \cos \frac{\bar{\omega}\bar{L}_{\pm}}{c_-} \right], \quad (\text{A11})$$

$$M(\bar{L}_{\pm}, \bar{\omega}, 3, 4) = \mp \frac{(c_+^2 - 1)(c_-^2 - 1)\bar{\omega}}{c_+c_-(c_+^2 - c_-^2)} \left[c_- \sin \frac{\bar{\omega}\bar{L}_{\pm}}{c_+} - c_+ \sin \frac{\bar{\omega}\bar{L}_{\pm}}{c_-} \right], \quad (\text{A12})$$

$$M(\bar{L}_{\pm}, \bar{\omega}, 4, 1) = \frac{\mp c_+^2 c_-^2}{(c_+^2 - c_-^2)} \left[\cos \frac{\bar{\omega}\bar{L}_{\pm}}{c_+} - \cos \frac{\bar{\omega}\bar{L}_{\pm}}{c_-} \right], \quad (\text{A13})$$

$$M(\bar{L}_{\pm}, \bar{\omega}, 4, 2) = \frac{\bar{\omega}}{(c_+^2 - c_-^2)} \left[c_+^3(c_-^2 - 1) \sin \frac{\bar{\omega}\bar{L}_{\pm}}{c_+} - c_-^3(c_+^2 - 1) \sin \frac{\bar{\omega}\bar{L}_{\pm}}{c_-} \right], \quad (\text{A14})$$

$$M(\bar{L}_{\pm}, \bar{\omega}, 4, 3) = \mp \frac{c_+^2 c_-^2}{(c_+^2 - c_-^2)\bar{\omega}} \left[c_+ \sin \frac{\bar{\omega}\bar{L}_{\pm}}{c_+} - c_- \sin \frac{\bar{\omega}\bar{L}_{\pm}}{c_-} \right], \quad (\text{A15})$$

$$M(\bar{L}_{\pm}, \bar{\omega}, 4, 4) = \frac{-1}{(c_+^2 - c_-^2)} \left[c_+^2(c_-^2 - 1) \cos \frac{\bar{\omega}\bar{L}_{\pm}}{c_+} - c_-^2(c_+^2 - 1) \cos \frac{\bar{\omega}\bar{L}_{\pm}}{c_-} \right]. \quad (\text{A16})$$

¹E. Yablonovitch, Phys. Rev. Lett. **58**, 2059 (1987).

²S. John, Phys. Rev. Lett. **58**, 2486 (1987).

³E. Yablonovitch, T. J. Gmitter, and R. Bhat, Phys. Rev. Lett. **61**, 2546 (1988).

⁴E. Yablonovitch and T. J. Gmitter, Phys. Rev. Lett. **63**, 1950 (1989).

⁵K. M. Ho, C. T. Chan, and C. M. Soukoulis, Phys. Rev. Lett. **65**, 3152 (1990).

⁶V. Karathanost, A. Modinos, and N. Stefanou, J. Phys.: Condens. Matter **6**, 6257 (1994).

⁷A. Moroz, Phys. Rev. B **66**, 115109 (2002).

⁸K. Busch and S. John, Phys. Rev. E **58**, 3896 (1998).

⁹S. Fan, P. R. Villeneuve, and J. D. Joannopoulos, Phys. Rev. B **54**, 11245 (1996).

¹⁰W. Y. Zhang, X. Y. Lei, Z. L. Wang, D. G. Zheng, W. Y. Tam, C. T. Chan, and P. Sheng, Phys. Rev. Lett. **84**, 2853 (2000).

- ¹¹M. S. Kushwaha, P. Halevi, L. Dobrzynski, and B. Djafari-Rouhani, *Phys. Rev. Lett.* **71**, 2022 (1993).
- ¹²M. M. Sigalas and E. N. Economou, *Solid State Commun.* **86**, 141 (1993).
- ¹³J. V. Sánchez-Pérez, D. Caballero, R. Martínez-Sala, C. Rubio, J. Sánchez-Dehesa, F. Meseguer, J. Llinares, and F. Galvez, *Phys. Rev. Lett.* **80**, 5325 (1998).
- ¹⁴F. R. Montero de Espinosa, E. Jiménez, and M. Torres, *Phys. Rev. Lett.* **80**, 1208 (1998).
- ¹⁵Z. Y. Liu, X. X. Zhang, Y. W. Mao, Y. Y. Zhu, Z. Y. Yang, C. T. Chan, and P. Sheng, *Science* **289**, 1734 (2000).
- ¹⁶C. Goffaux, J. Sanchez-Dehesa, A. L. Yeyati, Ph. Lambin, A. Khelif, J. O. Vasseur, and B. Djafari-Rouhani, *Phys. Rev. Lett.* **88**, 225502 (2002).
- ¹⁷Yanqing Lu, Yongyuan Zhu, Yanfeng Chen, Shining Zhu, Naiben Ming, and Yijun Feng, *Science* **284**, 1822 (1999).
- ¹⁸Y. Y. Zhu, X. J. Zhang, Y. Q. Lu, Y. F. Chen, S. N. Zhu, N. B. Ming, *Phys. Rev. Lett.* **90**, 053903 (2003).
- ¹⁹K. Huang, *Proc. R. Soc. London, Ser. A* **208**, 352 (1951); M. Born and K. Huang, *Dynamical Theory of Crystal Lattices* (Oxford University Press, Oxford, 1954).
- ²⁰X. J. Zhang, R. Q. Zhu, J. Zhao, Y. F. Chen, and Y. Y. Zhu, *Phys. Rev. B* **69**, 085118 (2004).
- ²¹Y. Nakagawa *et al.*, *J. Appl. Phys.* **44**, 3969 (1973).